J. Fluid Mech. (2010), *vol.* 664, *pp.* 238–264. © Cambridge University Press 2010
doi:10.1017/S0022112010003757

Fano resonances in acoustics

STEFAN HEIN[1], WERNER KOCH[1]† AND LOTHAR NANNEN[2]

[1]Institut für Aerodynamik und Strömungstechnik, DLR Göttingen, 37073 Göttingen, Germany

[2]Institut für Numerische und Angewandte Mathematik, Universität Göttingen, 37083 Göttingen, Germany

(Received 6 April 2010; revised 5 July 2010; accepted 12 July 2010; first published online 26 October 2010)

In contrast to completely open systems, laterally confined domains can sustain localized, truly trapped modes with nominally zero radiation loss. These discrete resonant modes cannot be excited linearly by the continuous propagating duct modes due to symmetry constraints. If the symmetry of the geometry is broken the trapped modes become highly localized quasi-trapped modes which can interfere with the propagating duct modes. The resulting narrowband Fano resonances with resonance and antiresonance features are a generic phenomenon in all scattering problems with multiple resonant pathways. This paper deals with the classical scattering of acoustic waves by various obstacles such as hard-walled single and multiple circular cylinders or rectangular and wedge-like screens in a two-dimensional duct without mean flow. The transmission and reflection coefficients as well as the (complex) resonances are computed numerically by means of the finite-element method in conjunction with two different absorbing boundary conditions, namely the complex scaling method and the Hardy space method. The results exhibit the typical asymmetric Fano line shapes near the trapped-mode resonances if the symmetry of the geometry is broken.

Key words: acoustics, noise control, wave scattering

1. Introduction

In a series of papers (Hein, Hohage & Koch 2004; Duan *et al.* 2007; Hein *et al.* 2007; Hein & Koch 2008; Koch 2009), we computed resonances in various two- and three-dimensional open systems. Here an open system is defined as a domain of wave activity which extends to infinity in at least one direction. In these open resonators one distinguishes two kinds of resonances namely leaky-mode resonances, so-called complex resonances which radiate energy to infinity, and localized trapped-mode resonances or bound-state resonances which nominally experience zero radiation loss. In acoustics, truly trapped modes with real resonant frequencies are possible only for laterally bounded domains such as waveguides or cascades; see e.g. Evans & Linton (1991) or Porter & Evans (1999). For Neumann boundary conditions on the bounding walls, Evans, Levitin & Vassiliev (1994) proved the existence of (at least) one trapped mode (antisymmetric about the centreline of the waveguide and with a resonant frequency below the cutoff frequency of the first duct crossmode) for a wide range of obstacles which are symmetric about the axis of a two-dimensional

† Email address for correspondence: werner.koch@dlr.de

https://doi.org/10.1017/S0022112010003757 Published online by Cambridge University Press

waveguide. Later on Davies & Parnovski (1998) established more conditions necessary as well as sufficient for the existence of trapped modes. Because of the asymmetry about the centreline of the waveguide, these trapped modes can be excited easily by localized sources, such as unstable shear layers, often leading to dangerous large-amplitude oscillations (see for example the review by Parker & Stoneman 1989). Essentially, all the resonance papers cited above are aimed at such localized excitation mechanisms.

On the other hand, these trapped modes cannot be excited linearly by propagating duct modes due to symmetry constraints (nevertheless, Li & Mei 2006 showed that trapped modes may be excited nonlinearly). However, Aslanyan, Parnovski & Vassiliev (2000) demonstrated that, if the symmetry of the geometry is broken, then a truly trapped mode becomes a slightly damped complex resonance. These highly localized quasi-trapped modes can interfere with propagating duct modes, causing dramatic changes in the sound transmission spectrum. We show here that these dramatic changes are due to Fano resonances, which are a generic feature in all scattering problems with multiple resonant pathways.

Fano (1935) (see also the recent English translation by Fano *et al.* 2005) was the first to publish a theoretical explanation for this interaction between a discrete quasi-trapped mode and a continuous-spectrum propagating mode when he studied autoionization in atoms. The results became widely known via his subsequent more elaborated publication Fano (1961), which is one of the most influential papers of 20th-century physics with more than 5700 citations by July 2010 (see the excellent review by Miroshnichenko, Flach & Kivshar 2010). The reason for this enormous impact is that Fano resonances with resonance and antiresonance features are a generic phenomenon in many different fields of physics and are not limited to quantum mechanics. For example, Joe, Satanin & Kim (2006) showed analogous resonance phenomena in a mechanical system consisting of an harmonically forced mass-spring oscillator linearly coupled to another oscillator, elucidating clearly the sharp amplitude suppression at antiresonance. On the basis of the analogy between scattering properties of electrons and phonons, El Boudouti *et al.* (2008) demonstrated that Fano resonances also exist in acoustical waveguides. Using one-dimensional theory (wavelength much larger than the duct width), they computed asymmetric as well as symmetric Fano resonances in a duct with side branches (see also the analogous problem in a quantum waveguide by Shao, Porod & Lent 1994 or in an optical waveguide by Mingaleev, Miroshnichenko & Kivshar 2008). If the wavelength is of the order of the duct width, a two-dimensional analysis is necessary requiring inevitably a numerical treatment as exemplified by Voo & Chu (2006).

In this paper we perform such a numerical analysis of the transmission and reflection of acoustic waves by various obstacles in a two-dimensional duct without mean flow demonstrating the existence of Fano resonances in the vicinity of quasi-trapped-mode frequencies. Whereas Fano resonances in semiconductor, photonic and phononic crystals are introduced by defects breaking the translational symmetry, the Fano resonances in our waveguide problem are due to asymmetry in the geometry. In this context, note that Fano resonances are also the basis for designing metamaterials (see for example Fedotov *et al.* 2007). Mimicking the quantum-mechanical phenomenon of electromagnetically induced transparency, quasi-trapped modes of coupled microresonators are used to achieve the necessary high quality factors Q (that is, the resonant frequency over the width of the resonance). The corresponding localized quasi-trapped modes, which are only weakly coupled to the free space, are generated from truly trapped modes by introducing slight asymmetries

https://doi.org/10.1017/S0022112010003757 Published online by Cambridge University Press

in the shape of the structural elements. Examples are the asymmetrically split rings of Fedotov *et al.* (2007) and Al-Naib, Jansen & Koch (2009) or the fish-scale pattern of Papasimakis, Fedotov & Zheludev (2008).

For the solution of transmission–reflection problems, various methods exist including powerful analytical methods (see for example Boström 1980, Linton & Evans 1992 or Linton 1995), as well as numerical methods such as boundary element methods (BEM), finite element methods (FEM) or hybrid methods; see Kirby (2008) and references therein. Another important tool for the solution of scattering problems is the scattering matrix method where the complex resonances appear as poles of the meromorphic continuation of the scattering matrix (see Borthwick 2007). In the recent publication Cattapan & Lotti (2007), an impurity in a multi-modal quantum waveguide is treated via this method. In this paper, we use the FEM in connection with two different formulations of absorbing boundary conditions, namely complex scaling and the Hardy space method, in order to solve the homogeneous resonance problem as well as the inhomogeneous scattering problem numerically for various different obstacle geometries.

This paper is structured as follows. In § 2 the resonance and scattering problem is formulated and the numerical solution method is outlined. Section 3 treats the scattering of acoustic waves by a single as well as multiple circular cylinders in a duct, demonstrating the appearance of Fano resonances as the symmetry with respect to the centreline of the waveguide is broken. In § 4 we discuss recently published results about acoustic screens and show that the observed narrowband high transmission losses are due to Fano resonances. We conclude with § 5 giving a brief summary.

2. Outline of the solution method

To locate the frequencies of possible Fano resonances, we need to compute the resonances and search for trapped or quasi-trapped modes. This means that in addition to the inhomogeneous scattering problem, we also have to solve the homogeneous resonance problem. Acoustic disturbances in an infinitely long duct of uniform height h^* with zero mean flow and containing an arbitrary object are governed by the wave equation, the propagation velocity being the ambient speed of sound c_0^*. Here, and in the following, the asterisk marks dimensional quantities. We formulate our problems in two-dimensional Cartesian coordinates (x, y) non-dimensionalized with a characteristic reference length l_{ref}^*, which in our waveguide examples is chosen to be the duct height h^* such that $h = h^*/l_{ref}^* = 1$. All velocities are non-dimensionalized with c_0^*, densities with the ambient density ρ_0^* and pressures with $\rho_0^* c_0^{*2}$. Assuming harmonic time dependence $\exp(-\mathrm{i}\omega^* t^*)$, where ω^* is the circular frequency, the wave equation in two dimensions reduces to the non-dimensional Helmholtz equation,

$$(\partial^2/\partial x^2 + \partial^2/\partial y^2 + K^2)\phi = 0, \tag{2.1}$$

for the velocity potential $\phi(x, y)$. The dimensionless frequency is defined as $K = \omega^* l_{ref}^*/c_0^*$, with $K/2\pi$ being the Helmholtz number. The time-independent dimensionless disturbance velocity and pressure are then given by $\boldsymbol{v}(x, y) = \nabla\phi$ and $p(x, y) = \mathrm{i}K\phi$, respectively.

On the sound-hard walls of the duct as well as the bounding surface of the objects in the duct, we prescribe Neumann boundary conditions

$$\frac{\partial\phi}{\partial n} = 0. \tag{2.2}$$

https://doi.org/10.1017/S0022112010003757 Published online by Cambridge University Press

In a uniform waveguide, the solution to (2.1) is in the form of duct modes

$$\phi(x, y) = \sum_{n=0}^{\infty} \{A_n \mathrm{e}^{\mathrm{i}K_n x} + B_n \mathrm{e}^{-\mathrm{i}K_n x}\} \cos\{n\pi(y + h/2)/h\}, \tag{2.3}$$

where A_n, B_n are the (complex) modal amplitudes of waves travelling in the $+x$ and $-x$ directions, respectively. The modal wavenumber $K_n = \{K^2 - (n\pi/h)^2\}^{1/2}$ with positive real part denotes a propagating wave for $K > (n\pi/h)$, otherwise the wave is evanescent (cutoff) (in scattering theory, one speaks of open and closed channels, respectively). For the scattering problem, the frequency K is prescribed and the solution is written as sum of the incoming wave $\phi^{(i)}$ and the scattered wave $\phi^{(s)}$:

$$\phi(x, y) = \phi^{(i)}(x, y) + \phi^{(s)}(x, y). \tag{2.4}$$

The incoming wave $\phi^{(i)}$ is given in the modal form as

$$\phi^{(i)}(x, y) = E_r \mathrm{e}^{\mathrm{i}K_r x} \cos\{r\pi(y + h/2)/h\}, \tag{2.5}$$

with E_r being the prescribed amplitude of the rth incoming propagating mode. The scattered wave $\phi^{(s)}$ is then the solution to a radiation problem with prescribed normal derivative on the bounding surface of the scatterer annihilating the normal derivative caused by the incoming wave. The formulation of the scattering problem is completed by imposing a radiation condition allowing only outgoing waves, i.e. waves with positive energy flux coming from the scatterer. This guarantees that the scatterer is the source of a wave travelling to infinity.

Using the complex velocity potential ϕ, the energy flux through a cross-section Γ of the waveguide is given by (see for example Pierce 1981, p. 40)

$$\frac{1}{2} \mathrm{Re}\left\{ \int_\Gamma \overline{p^{(s)}} \boldsymbol{v}^{(\mathbf{s})} \cdot \mathrm{d}\boldsymbol{\Gamma} \right\} = \pm \frac{K}{2} \mathrm{Im}\left\{ \int_{-h/2}^{h/2} \overline{\phi^{(s)}(x, y)} \frac{\partial \phi^{(s)}(x, y)}{\partial x} \, \mathrm{d}y \right\}. \tag{2.6}$$

The sign $\pm$ depends on the orientation of Γ in the $+x$ or $-x$ direction. The propagating modes (K_n real and positive) in (2.3) with $\exp(\mathrm{i}K_n x)$ are outgoing in the $+x$ direction, while the modes with $\exp(-\mathrm{i}K_n x)$ are outgoing in the $-x$ direction. The cutoff modes do not contribute to the energy flux, but the same classification can be used for the cutoff modes because for $\mathrm{Im}(K_n) > 0$ the modes with $\exp(\pm \mathrm{i}K_n x)$ are exponentially decreasing for $x \to \pm\infty$.

For the resonance problem, we obtain the frequency K as solution of an eigenvalue problem (see Zworski 1999): we solve the eigenvalues K^2 with the corresponding radiating eigenfunctions ϕ which satisfy the Helmholtz equation (2.1) together with vanishing Neumann boundary conditions on the duct and obstacle walls. In other words, we compute the (complex) resonances K with positive real part for which the homogeneous problem (no incoming wave) has non-trivial solutions (a similar approach is often used to prove the existence of trapped modes). We call $\mathrm{Re}(K)$ the resonant frequency, ϕ the resonant function and $|\mathrm{Im}(K)|$ the damping. From this, the quality factor

$$Q = \mathrm{Re}(K)/(2|\mathrm{Im}(K)|) \tag{2.7}$$

of a resonance can be computed and this is proportional to the ratio of stored energy over energy loss per cycle.

Historically, resonances were often defined as large response of an oscillating system to a given source. A resonance defined this way depends on the source and the

https://doi.org/10.1017/S0022112010003757 Published online by Cambridge University Press

objective function. For example, using (2.6) we can compute the energy reflection and transmission factors τ_r and ρ_r which are defined as the ratio between the transmitted (or reflected) energy and the energy of a prescribed rth incoming wave. The frequency of the transmission resonance is usually different from the frequency of the reflection resonance and cannot be computed directly from the resonance. The dependency of the response on the source can be demonstrated very clearly for a symmetric obstacle in a duct: the response to an incoming plane wave at the trapped-mode frequency is zero whereas the response to vortex excitation (or equivalently two loudspeakers in the opposite duct walls and phase-shifted by π, see for example the similar excitation in Aly & Ziada 2010) is very large. Therefore, we prefer the eigenvalue approach, which gives a unique definition of the resonant frequencies. Numerically, we truncate the unbounded waveguide by artificial boundaries, creating a bounded domain which can be discretized by FEM. In this paper, we apply the high-order code NGSolve of Joachim Schöberl, together with his grid generation code NETGEN; cf. Schöberl (1997). The resulting matrix eigenvalue problem is solved using a shifted Arnoldi algorithm. The accuracy of the finite-element solution is controlled by the maximal mesh size Δ of the grid and the order p of the finite element polynomial on an individual triangle. In NGSolve, the mesh size Δ can be varied locally.

The implementation of the radiation condition needs special attention because at the artificial boundaries unphysical reflections occur unless special boundary conditions are applied. Basically there are two methods to overcome this problem: the first uses the so-called non-reflecting boundary conditions on the surface bounding the computational domain. They are approximations to the so-called Dirichlet-to-Neumann (DtN) operator, mapping the Dirichlet values of the unknown solution on the artificial boundary onto their Neumann values. Because of (2.3), this mapping is given by mapping the modal amplitudes A_n in the $+x$ direction and B_n in the $-x$ direction to the amplitudes $\mathrm{i}K_nA_n$ and $-\mathrm{i}K_nB_n$, respectively. Since the cutoff waves decay exponentially in n, a simple approximation to the exact DtN operator uses only the first N modes (see for example Harari, Patlashenko & Givoli 1998). Such a boundary condition depends nonlinearly on K because K_n depends nonlinearly on K. In the case of the resonance problem, this leads to a nonlinear eigenvalue problem and is therefore not advisable.

The second class of methods consists of a special treatment of the unbounded domain outside the bounded computational domain. For our numerical analysis we use two different methods of this kind: the scattering problem is solved using the so-called Hardy space method of Nannen (2008), Hohage & Nannen (2009) and Nannen & Schädle (2010). The method has been implemented by Lothar Nannen in the high-order finite element code NGSolve of Joachim Schöberl (cf. Schöberl 1997) and relies on the fact that the Laplace transform of an outgoing solution to the Helmholtz equation belongs to a certain Hardy space, while an incoming solution does not. Hence, using special finite element basis functions out of this Hardy space guarantees that the solution is outgoing. Although the theoretical justification and the implementation of the method is complicated, it is very easy to use. Only the number of degrees of freedom in the unbounded domain and a parameter depending on K have to be chosen. The Hardy space method depends linearly on K^2 and therefore leads to a linear eigenvalue problem for the resonance problem.

Nevertheless, we use the complex scaling method for the solution of the resonance problem because it not only leads to a linear eigenvalue problem for K^2 but also has

https://doi.org/10.1017/S0022112010003757 Published online by Cambridge University Press

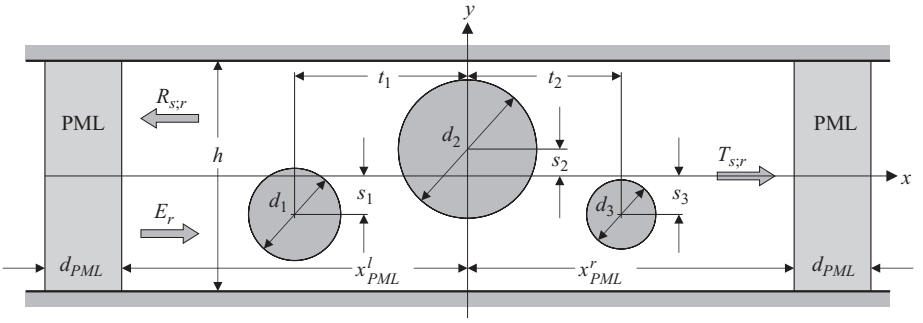


FIGURE 1. Sketch of acoustic scattering by multiple circular cylinders off-centre in a two-dimensional duct with PMLs.

the advantage that it is well established in the atomic and molecular physics literature. It adds a non-physical layer to the computational domain in which outgoing waves are absorbed (therefore, some authors use the term absorbing boundary conditions). A perfectly matched layer (PML) is a refined absorbing layer introduced by Bérenger (1994) with no spurious reflections at the PML interface due to perfect impedance matching (however, weak reflections are possible due to numerical discretization). The PML method of Bérenger (1994) became increasingly popular in numerically solving electromagnetic and acoustic problems in open domains (for a recent review in acoustics see Hu 2004). Instead of the frequency-dependent PML formulation of Bérenger (1994) in the form of the complex coordinate stretching formulation of Chew & Weedon (1994), Hein *et al.* (2004) used the much older complex scaling method of atomic and molecular physics with frequency-independent PML coefficients. For the scattering problem with a prescribed real frequency, the complex scaling method and the PML method of Bérenger (1994) are essentially identical because the real frequency only rescales the PML parameter. For the resonance problem, the PML method of Bérenger (1994) leads to a nonlinear eigenvalue problem. Therefore, in the few resonance problems treated by the PML method of Bérenger (1994), in the literature usually the frequency ω is fixed in the PML formulation by a reference frequency ω_0 in the range of interest (see for example Bindel & Govindjee 2005). This way a linear eigenvalue problem results and the formulation again corresponds to the complex scaling method.

The complex scaling method, also termed the Aguilar–Baslev–Combes–Simon theory, was introduced by Aguilar & Combes (1971), Baslev & Combes (1971) and Simon (1973); see the monograph by Hislop & Sigal (1996) or the recent review by Moiseyev (1998). It makes use of the fact that the PML eigenvalues for the infinite domain problem coincide with the resonances of the original problem for rather general PML scalings. In a recent paper Kim & Pasciak (2009) proved that the eigenvalues of the truncated PML problem (a necessity for the numerical approach) converge to the desired resonances as the PML domain increases. The complex scaling method works as follows: in the PML domain (see figure 1), $\phi(x, y)$ is continued analytically with respect to the axial variable x to the complex variable ξ, e.g.

$$\xi(x) = x + \mathrm{i}\sigma(x). \tag{2.8}$$

The spatial damping function $\sigma(x)$ is usually chosen in power form, smoothly starting

https://doi.org/10.1017/S0022112010003757 Published online by Cambridge University Press

at the PML interfaces at $x = x^r_{PML}$ and $x = x^l_{PML}$, respectively:

$$\sigma(x) = \begin{cases} \sigma_0 (x - x^r_{PML})^\beta, & x > x^r_{PML}, \\ 0, & -x^l_{PML} \leqslant x \leqslant x^r_{PML}, \\ -\sigma_0 (-x - x^l_{PML})^\beta, & x < -x^l_{PML}. \end{cases} \tag{2.9}$$

For a positive damping coefficient σ_0 and a constant shape parameter $\beta \geqslant 1$, outgoing waves will decay exponentially in the PML. One can therefore truncate the PML at $(x^r_{PML} + d_{PML})$ and $-(x^l_{PML} + d_{PML})$, where d_{PML} denotes the width of the PML. The error due to artificial reflections at this truncated outer edge of the PML is small if σ_0 and d_{PML} are chosen properly (in general, we chose $\beta = 1$, $\sigma_0 = 1$ and $d_{PML} \geqslant 2$). Therefore, a Dirichlet boundary condition can be imposed at the outer edge of the PML instead of enforcing the radiation condition; cf. Collino & Monk (1998).

3. Scattering by circular cylinders in a duct

In this section we consider the classical problem of sound scattering by circular cylinders placed in a two-dimensional duct as sketched schematically in figure 1. The incoming multi-modal sound is prescribed in terms of the modal amplitudes E_r of the propagating duct modes; see Kirby (2008). However, in this paper we limit ourselves to a single incoming mode E_r, as given by (2.5). Then, the amplitude of the sth reflected and transmitted mode due to the rth incident mode is denoted by $R_{s;r}$ and $T_{s;r}$, respectively, and the modal energy reflection and transmission coefficients are defined by

$$\rho_{s;r} = \frac{(2 - \delta_{r,0}) K_s}{(2 - \delta_{s,0}) K_r} \left| \frac{R_{s;r}}{E_r} \right|^2, \quad \tau_{s;r} = \frac{(2 - \delta_{r,0}) K_s}{(2 - \delta_{s,0}) K_r} \left| \frac{T_{s;r}}{E_r} \right|^2. \tag{3.1}$$

Here, $\delta_{m,n}$ denotes Kronecker's delta function. The total energy reflection and transmission coefficients ρ_r and τ_r due to a single incoming mode r are then obtained by summing the above-defined modal reflection and transmission coefficients over all propagating modes s. Conservation of energy requires

$$\rho_r + \tau_r = 1, \tag{3.2}$$

which allows an excellent check of the numerical accuracy. In our computations, we do not use the modal coefficients (3.1) but compute the total energy reflection and transmission coefficients directly by using (2.6). In noise control, usually the so-called transmission loss TL (in decibels) is used, and this is defined by

$$TL\,(\mathrm{dB}) = 10 \log_{10}(1/\tau_r). \tag{3.3}$$

Before investigating the scattering problem, we compute the resonances and herewith the quality factors Q of the individual resonances and their dependence on various geometry parameters in order to see where Fano resonances can be expected.

3.1. *Resonances of a single circular cylinder in a duct*

First, we consider the classical problem of a single circular cylinder centred in the duct with $s/h = 0$ and vary the diameter d/h of the circular cylinder. Here s denotes the distance by which the cylinder is offset from the duct axis as sketched in figure 1. Because of symmetries in the geometry, we can limit ourselves to solving the quarter problem $x \geqslant 0$, $y \geqslant 0$. The results are shown in figure 2, where figure 2(a) gives the resonant frequency $\mathrm{Re}(K/2\pi)$ and figures 2(b) and 2(c) show the damping $\mathrm{Im}(K/2\pi)$ of the y-antisymmetric and y-symmetric resonances, respectively. For $s/h = 0$, truly

https://doi.org/10.1017/S0022112010003757 Published online by Cambridge University Press

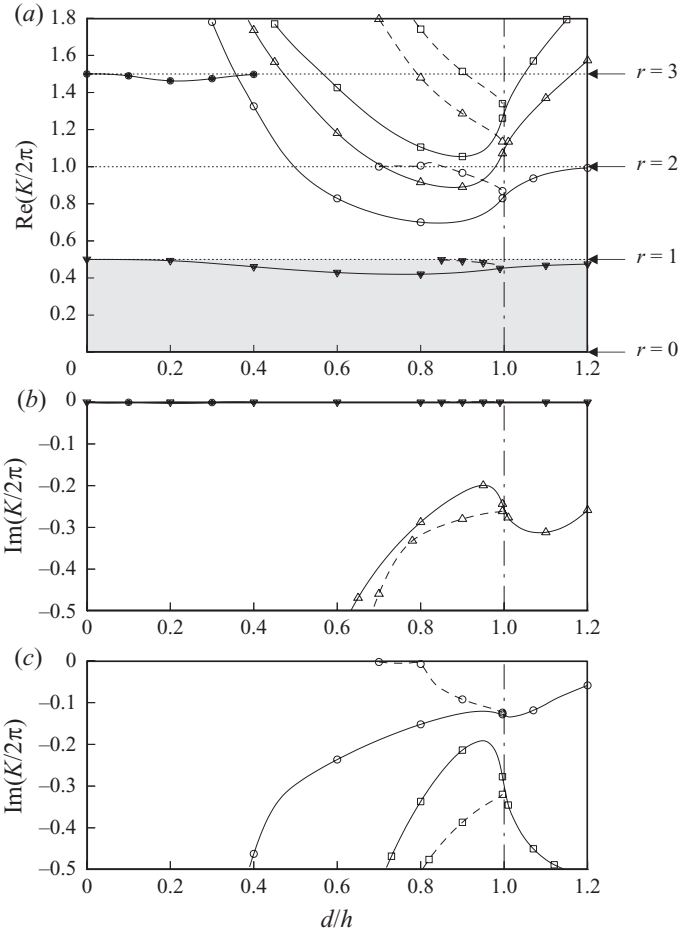


FIGURE 2. Acoustic resonances of a circular cylinder centred in a two-dimensional duct ($s/h = 0$): effect of cylinder diameter d/h. (*a*) Resonant frequency, (*b*) damping of *y*-antisymmetric resonances and (*c*) damping of *y*-symmetric resonances. Solid lines denote *x*-symmetric resonances and dashed lines denote *x*-antisymmetric resonances. The arrows on the right mark the cutoff frequencies of the duct. $p = 10$, $d_{PML} = 3$, $\Delta = 0.08$ and various σ_0.

trapped modes exist below the cutoff frequency of the first duct crossmode (indicated by the shaded domain in figure 2*a*) as proved by Evans *et al.* (1994) (see also the computations of Callan, Linton & Evans 1991 or Duan *et al.* 2007). These trapped modes are marked by solid triangles in figure 2 and are antisymmetric about the centreline of the duct. The *x*-symmetric modes are shown by solid lines, and *x*-antisymmetric modes are shown by dashed lines. The *x*-antisymmetric trapped modes exist only in a narrow region $0.81 < d/h < 1$ as shown by Evans & Porter (1999). Experimental confirmations of these trapped modes for the equivalent water wave problem were published by Retzler (2001) and Cobelli *et al.* (2009). At $d/h = 1$ (marked by the dash-dotted line), the cylinder touches the duct walls and for $d/h > 1$ separates the duct into two independent semi-infinite domains. At $d/h = 1$, our grid generation code fails but the *x*-symmetric and *x*-antisymmetric branches appear to coincide there, which is plausible because for $d/h > 1$ the notion of symmetry and antisymmetry in x is lost as noted by Porter (2007) for a similar elastic wave problem.

https://doi.org/10.1017/S0022112010003757 Published online by Cambridge University Press

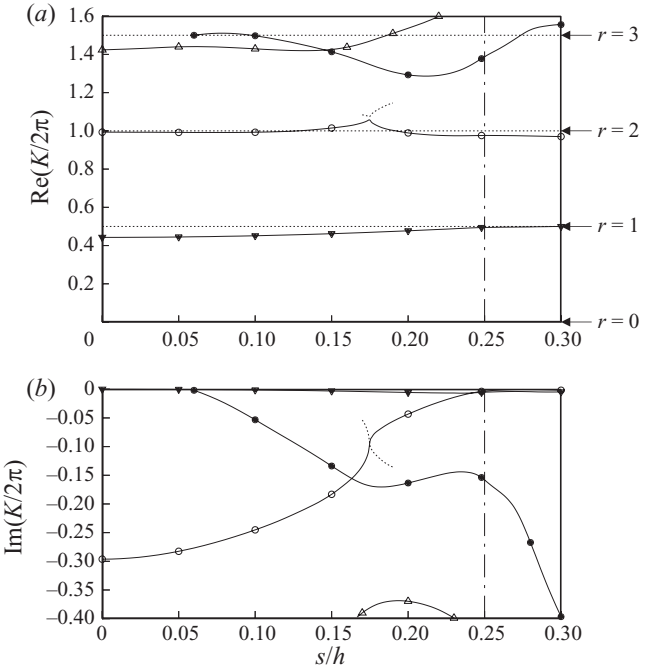


FIGURE 3. Acoustic resonances of a circular cylinder with $d/h = 0.5$ in a two-dimensional duct of width h: effect of off-centre distance s/h. (a) Resonant frequency and (b) damping. The arrows on the right mark the cutoff frequencies of the duct. $p = 10$, $d_{PML} = 4$, $\Delta = 0.16$ and various σ_0.

Cobelli *et al.* (2009) observed that for $d/h > 1$ the trapped mode in figure 2 becomes an edge mode exponentially decaying away from the cylinder. A nearly trapped mode below the cutoff frequency of the second duct crossmode at $K/2\pi = 1.5$ is marked by solid circles in figure 2. This mode has a node between the cylinder and the duct wall, and Evans & Porter (1998) (see also Duan *et al.* 2007) showed that even an isolated embedded trapped mode exists on that curve for the particular value of $d/h = 0.35209$.

All the above-mentioned trapped modes are antisymmetric about the centreline of the duct and therefore cannot be excited by the fundamental duct mode with amplitude E_0, which is symmetric about $y = 0$. However, as can be seen from figure 2 other highly damped scattering modes exist, which are marked by open symbols. Here, open circles and squares denote highly damped scattering modes symmetric about the duct axis $y = 0$ and open triangles mark those antisymmetric about $y = 0$. In figure 2(b) we plotted the damping of the first highly damped y-antisymmetric scattering mode in addition to the trapped modes with zero damping, and in figure 2(c) we included the first two highly damped y-symmetric scattering modes. We note that the highly damped scattering resonances also have x-symmetric and x-antisymmetric branches, which seem to converge near $d/h = 1$ similar to the trapped-mode resonance.

Next, we fix $d/h = 0.5$ and compute the resonances as a function of s/h. Now we have only symmetry about the y-axis and therefore consider the half problem $x \leqslant 0$. The results are shown in figure 3, where we have used the same symbols at $s/h = 0$ as in figure 2 to identify corresponding modes. As soon as $s/h \neq 0$, the trapped mode of figure 2, marked by the filled triangle, becomes a slightly damped

https://doi.org/10.1017/S0022112010003757 Published online by Cambridge University Press

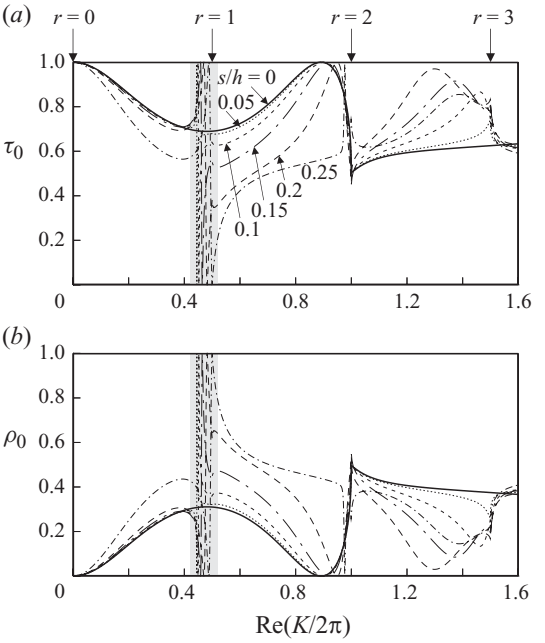


FIGURE 4. Transmission and reflection coefficients of a circular cylinder with $d/h = 0.5$ in a two-dimensional duct of width h: effect of off-centre distance s/h. (*a*) Transmission coefficient τ_0 and (*b*) reflection coefficient ρ_0. The arrows on top mark the cutoff frequencies of the duct and the shaded domain outlines the frequency range near the Fano resonances.

quasi-trapped mode whereas all other modes are highly damped. Near $s/h = 0.173$, a marked peak appeared in the frequency of the first y-symmetric resonant mode. Unfortunately, this is near the continuous spectrum of the second y-symmetric duct mode where the accuracy of our resonance computation is rather low. Nevertheless, more detailed computations with $\sigma_0 = 0.25$ and $d_{PML} = 8$ showed that a second solution branch, depicted by the dotted curve in figure 3, approaches the first y-symmetric resonant mode near this peak. This second solution branch appears to be on a different Riemann sheet and non-physical because it does not show up as a second maximum in the transmission coefficient. Furthermore, the unphysical solution ends at $s/h = 0.25$, where the cylinder touches the upper wall.

3.2. *Reflection and transmission coefficients of a single circular cylinder in a duct*

After locating the quasi-trapped-mode resonances for $d/h = 0.5$ in figure 3, we know where to look for Fano resonances. First, we compute the transmission coefficient τ_0 and the reflection coefficient ρ_0 for an incoming fundamental mode impinging on a centred cylinder with $s/h = 0$. These computations can be compared with the multipole results published by Linton & Evans (1992) in their figure 7. Our numerical results for $s/h = 0$ are shown in figure 4 by the thick solid curve. We observe a transmission resonance near $\mathrm{Re}(K/2\pi) = 0.89$, which stems from the highly damped resonance near $\mathrm{Re}(K/2\pi) = 1.0$ in figure 2. Note that the resonant frequency $\mathrm{Re}(K/2\pi)$ does not coincide with the frequency of peak transmission, which is lower than the resonant frequency (for an harmonically excited damped oscillator, the relation between resonant frequency and frequency of peak response can be given explicitly in terms of the damping). With $s/h > 0$, the imaginary part of this resonance, marked

https://doi.org/10.1017/S0022112010003757 Published online by Cambridge University Press

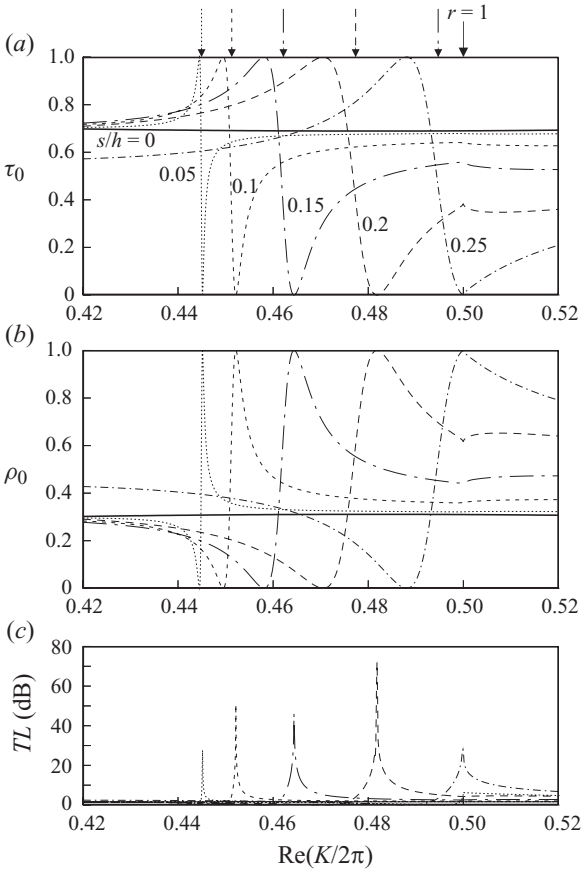


FIGURE 5. Expanded view of the frequency range $0.42 \leqslant \mathrm{Re}(K/2\pi) \leqslant 0.52$ shaded in figure 4: (*a*) transmission coefficient τ_0, (*b*) reflection coefficient ρ_0 and (*c*) transmission loss TL.

by open circles in figure 3, closely approaches zero near $s/h = 0.25$. For this almost undamped resonance, the transmission maximum is near the resonant frequency.

For $s/h > 0.05$, a second transmission maximum shows up in figure 4 between $\mathrm{Re}(K/2\pi) = 1$ and 1.5, which is due to the second damped resonance marked by solid circles in figure 3. With increasing s/h, this transmission maximum moves to lower frequencies up to about $s/h = 0.2$ as does the corresponding resonance. For $s/h > 0.2$, the resonant frequency increases again and consequently the transmission maximum also moves to higher frequencies as can be seen for the $s/h = 0.25$ example in figure 4. In figure 8 of Linton & Evans (1992) for $d/h = 0.9$ as well as in figure 10 of Kirby (2008) for $d/h = 0.8$, we note that the transmission coefficient has two maxima below $\mathrm{Re}(K/2\pi) = 1$. From our figure 2 it seems that this second maximum is generated by the weakly damped x-antisymmetric (but y-symmetric) resonance.

The most striking changes are due to Fano resonances near the quasi-trapped-mode resonances marked by the curve with solid triangular symbols in figure 3. As soon as $s/h \neq 0$, we note the appearance of a narrow frequency band near $\mathrm{Re}(K/2\pi) = 0.5$ in figure 4, where the transmission coefficient τ_0 first reaches a maximum and then a minimum corresponding to a transmission resonance and transmission antiresonance, respectively. The opposite occurs with the reflection coefficient ρ_0 as can be seen in figure 5, where the narrow frequency range around the frequency of the

https://doi.org/10.1017/S0022112010003757 Published online by Cambridge University Press

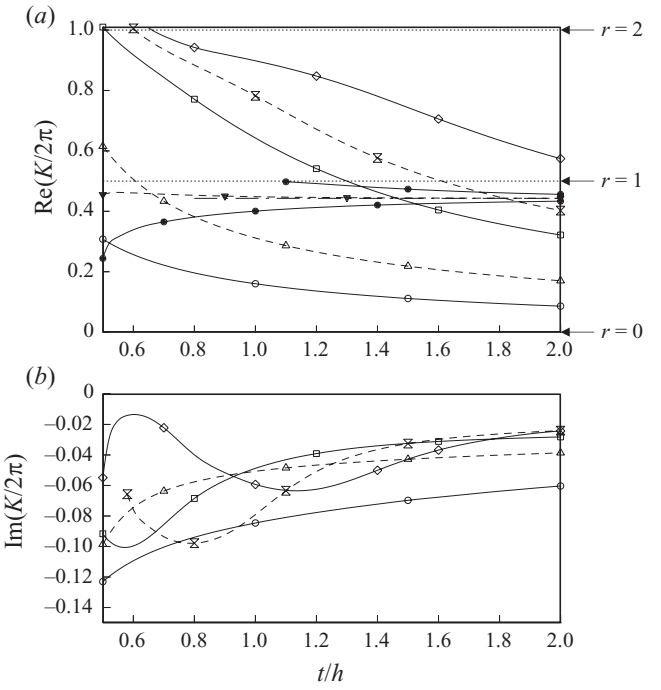


FIGURE 6. Acoustic resonances of three identical and equally spaced circular cylinders with $d/h = 0.5$ and $s/h = 0$ on the centreline of a duct of width h: effect of distance t/h between the cylinders. (a) Resonant frequency and (b) damping. Solid lines denote x-symmetric resonances and dashed lines denote x-antisymmetric resonances. $p = 10$, $d_{PML} = 4$, $\Delta = 0.16$ and various σ_0.

quasi-trapped-mode resonance, which is shaded in figure 4, is enlarged. Note that $\tau_0 + \rho_0$ is equal to 1 within an error of less than 10^{-8} in all our computations. Figure 5(c) shows the corresponding transmission loss TL which is of importance in noise control. With increasing s/h, the transmission maxima and minima of the Fano resonance move to slightly higher frequencies, a trend predicted by the quasi-trapped-mode resonances of figure 3. The asymmetric line shape of the resonance embedded in the background result for $s/h = 0$ is typical for a Fano resonance. Even though the damping of these quasi-trapped modes is very small, the resonant frequencies of figure 3, reshown by the unlabelled arrows on the top of figure 5(a), do not coincide with the maxima of the transmission coefficient.

3.3. *Resonances of multiple circular cylinders in a duct*

It is well known that for multiple obstacles in a duct, several truly trapped modes may exist with important implications on the acoustic design of flow compressors (see Parker 1984) or heat exchanger tube bundles (see Parker 1978). For example, Evans & Porter (1997) showed that for N circular cylinders with different diameters d_j, $j = 1, \ldots, N$, arbitrarily spaced with t_j, $j = 1, \ldots, N-1$, along the centreline of the duct with $s_j = 0$, $j = 1, \ldots, N$ (see figure 1), up to N truly trapped modes exist. The precise number of trapped modes depends crucially on the geometry (similar to the single cylinder case even more than N trapped modes are possible if d/h is sufficiently large). On the other hand, Utsunomiya & Eatock Taylor (1999) and Porter & Evans (1999) demonstrated that M truly trapped modes exist for a row of M circular cylinders equally spaced along a line perpendicular to the duct

https://doi.org/10.1017/S0022112010003757 Published online by Cambridge University Press

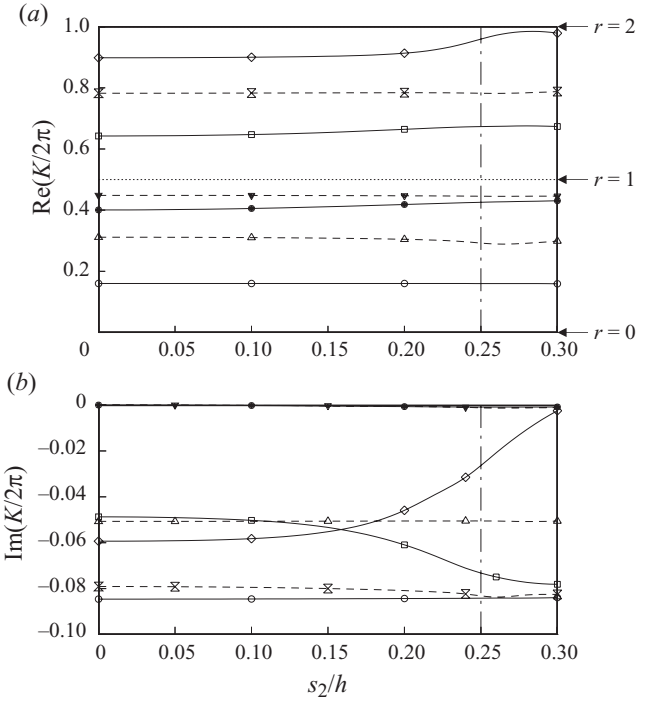


FIGURE 7. Acoustic resonances of three identical and equally spaced circular cylinders with $d/h = 0.5$ and $t/h = 1$ in a duct of width h: effect of lateral offset s_2/h. (a) Resonant frequency and (b) damping. Solid lines denote x-symmetric resonances and dashed lines denote x-antisymmetric resonances. $p = 10$, $d_{PML} = 4$, $\Delta = 0.16$ and various σ_0.

walls. Finally, Porter & Evans (2002) computed the trapped modes in a rectangular array of $N \times M$ cylinders placed in a waveguide and compared their results with those of Blevins (1986), who used homogenization theory. All these trapped-mode cases assume a geometry which is symmetric about the centreline of the duct (see also Linton & McIver 2002).

In this paper, we consider geometries where this symmetry is broken. There are different ways of achieving this. As a particular example, generalizing the single-cylinder case treated in the previous section, we consider three identical cylinders $d_1 = d_2 = d_3 = d = 0.5$, equally spaced with $t_1 = t_2 = t$ along the centreline of the duct and vary the lateral offset s_2 of the second cylinder keeping the first and third cylinders centred, e.g. $s_1 = s_3 = 0$. Starting with $s_2/h = 0$, we first show the resonances for variable t/h in figure 6. In agreement with the findings of Evans & Porter (1997), the frequencies of the trapped modes, shown by filled symbols in figure 6, approach the single-cylinder result of the previous section, shown by the dash-dotted line, as $t/h \to \infty$. At $t/h = 0.5$, the three cylinders touch each other and only two trapped modes, one x-symmetric and the other x-antisymmetric, exist. The third (x-symmetric) trapped mode only appears around $t/h \approx 1.1$. Aside from the trapped modes, damped mode resonances also exist. We marked the first five y-symmetric resonances by open symbols in figure 6. Of the y-antisymmetric modes only the trapped mode is shown. Again, solid lines indicate x-symmetric resonances and dashed lines indicate x-antisymmetric resonances.

Next, we fix $t/h = 1$, $d/h = 0.5$ and vary the lateral offset s_2/h of the second cylinder keeping $s_1 = s_3 = 0$. The results are shown in figure 7. Starting with $s_2/h = 0$ we use

https://doi.org/10.1017/S0022112010003757 Published online by Cambridge University Press

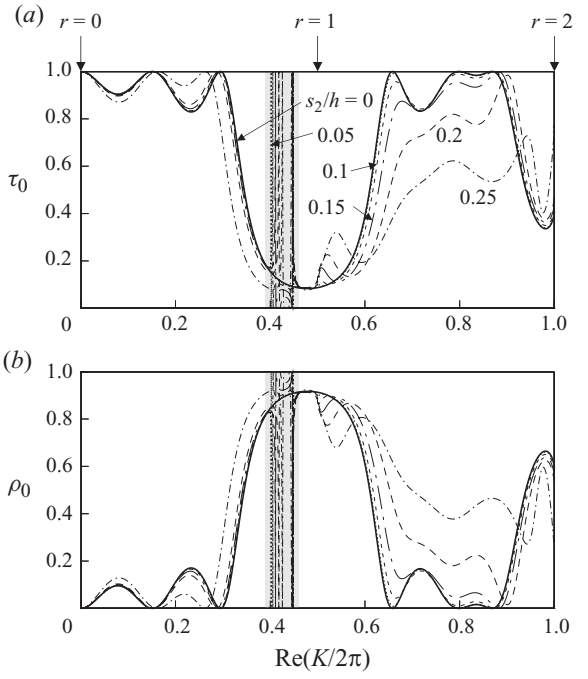


FIGURE 8. Transmission and reflection coefficients of three identical circular cylinders with $d/h = 0.5$ and $t/h = 1$ placed on the centreline of a duct of width h: effect of varying the offset s_2/h keeping $s_1 = s_3 = 0$. (*a*) Transmission coefficient τ_0 and (*b*) reflection coefficient ρ_0. The shaded domain outlines the frequency range near the Fano resonances.

the same symbols as in figure 6 to identify corresponding modes. For $s_2/h \neq 0$, the two trapped modes become highly localized quasi-trapped modes. The frequency of the x-symmetric quasi-trapped mode approaches the frequency of the x-antisymmetric quasi-trapped mode as s_2/h increases, whereas the latter remains fairly constant up to $s_2/h = 0.3$. At $s_2/h = 0$, there exist two strongly damped y-symmetric resonances, marked by open circular and triangular symbols in figure 7, below the trapped-mode frequencies and three strongly damped y-symmetric resonances, also marked by open symbols, above the frequencies of the trapped modes but below $\mathrm{Re}(K/2\pi) = 1$. These are most likely to be excited by a plane wave. The frequencies of these strongly trapped resonances stay fairly constant with s_2/h. Only the frequency of the resonance marked by open triangles decreases slightly with increasing s_2/h, whereas the frequency of the resonance marked by the open diamond symbol increases near $s_2/h = 0.25$, where the second cylinder starts penetrating the duct wall. All these trends will be checked in the next section by looking at the frequencies of the maxima of the transmission coefficient τ_0.

3.4. *Reflection and transmission coefficients of multiple circular cylinders in a duct*

In this section we compute the transmission and reflection coefficients τ_0 and ρ_0, respectively, for the above-treated example with $t/h = 1$ varying the lateral offset s_2/h of the second cylinder keeping $s_1 = s_3 = 0$. The results are shown in figure 8. The frequency region of the Fano resonances is shaded in figure 8 and replotted enlarged in figure 9. First, we look at the results for $s_2/h = 0$, shown by the thick solid curve in figure 8. As predicted by the damped resonances in figure 7, the transmission coefficient τ_0 has two maxima below the shaded Fano region in figure 8

https://doi.org/10.1017/S0022112010003757 Published online by Cambridge University Press

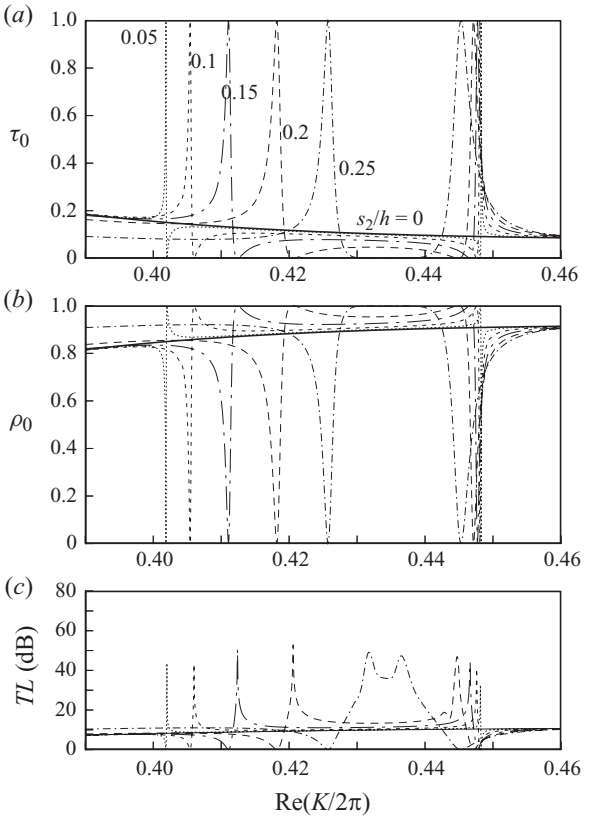


FIGURE 9. Expanded view of the frequency range $0.39 \leqslant \mathrm{Re}(K/2\pi) \leqslant 0.46$ shaded in figure 8: (*a*) transmission coefficient τ_0, (*b*) reflection coefficient ρ_0 and (*c*) transmission loss TL.

and after a large dip three more maxima below $\mathrm{Re}(K/2\pi) = 1$. This dip transforms into a phononic band gap if the number of cylinders increases. We note that at the frequencies of the two trapped modes, τ_0 has no maximum. With $s_2/h \neq 0$, the above maxima follow closely the trend predicted by the resonances in figure 7, especially the fifth maximum moves to higher frequencies with increasing s_2/h.

However, the most drastic change occurs near the frequencies of the two quasi-trapped modes if $s_2/h \neq 0$. As shown in more detail in figure 9, we observe two Fano resonances: the first starts off with a transmission maximum followed by a transmission minimum whereas the second starts off with a transmission minimum followed by a transmission maximum. With increasing s_2/h the frequency of the first Fano resonance moves towards the frequency of the second Fano resonance, as predicted by the resonances in figure 7. For $s_2/h = 0.25$, we observe a sizable region of high transmission loss in figure 9(*c*). Essentially, the two Fano resonances interact there. The small local maximum of τ_0 near $\mathrm{Re}(K/2\pi) = 0.5$ in figure 8 is due to a resonance originating from a *y*-antisymmetric resonance at $s_2/h = 0$.

4. Acoustic screens

We are unaware of any experiments demonstrating the existence of Fano resonances for circular cylinders in a duct. However, without mentioning Fano resonances, Rim & Kim (2000) recently showed that hard-walled screens of various geometries placed

https://doi.org/10.1017/S0022112010003757 Published online by Cambridge University Press

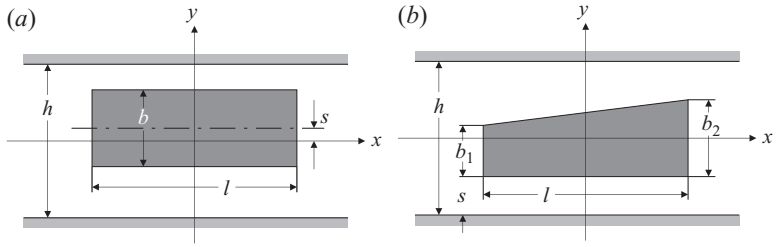


FIGURE 10. Sketch of (*a*) symmetric rectangular screen and (*b*) asymmetric screen off-centred by s in a two-dimensional duct.

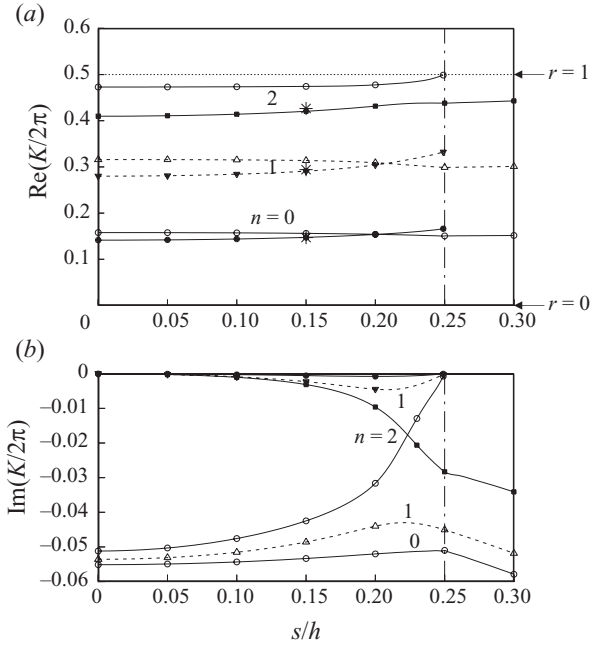


FIGURE 11. Acoustic resonances of a rectangular block with $l/h = 3$, $b/h = 0.5$ in a two-dimensional duct of width h: effect of off-centre displacement s/h. (*a*) Resonant frequency and (*b*) damping. The asterisks denote BEM results of Rim & Kim (2000) for peak transmission loss at $s/h = 0.15$. $p = 6$, $d_{PML} = 2(4)$, $\sigma_0 = 2$, $\Delta = 0.2$.

asymmetrically in a straight duct give rise to large narrowband sound attenuation. They argued correctly that due to path asymmetry higher-order evanescent modes are excited. On the basis of this finding, they developed a simple analytical model which they compared with extensive experiments and numerical BEM computations. The narrowband peaks of y-symmetric rectangular screens disappeared when the rectangular screen was centred on the axis of the duct. This is exactly the case for which Evans *et al.* (1994) proved that trapped modes exist with zero radiation loss. However, as soon as the symmetry of the problem with regard to the centre of the duct is broken, the trapped modes become complex resonances with radiation losses as shown by Aslanyan *et al.* (2000). (An exception to this is an infinitely thin plate of finite length for which trapped modes exist for any offset s/h; e.g. Evans 1992. The reason for this exception is that a thin plate does not scatter an incoming plane wave as noted by Linton *et al.* 2002.) Therefore, the narrowband attenuation can be linked

https://doi.org/10.1017/S0022112010003757 Published online by Cambridge University Press

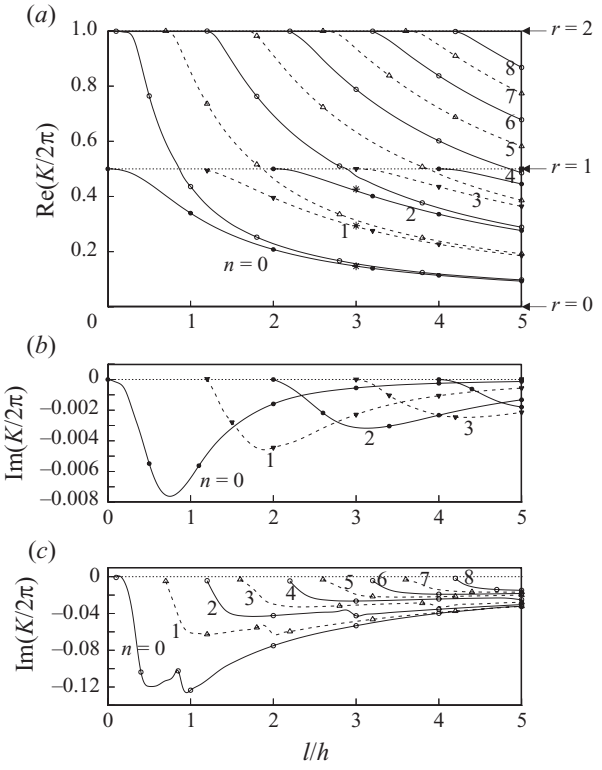


FIGURE 12. Acoustic resonances of a rectangular block with $b/h = 0.5$, $s/h = 0.15$ in a two-dimensional duct of width h: effect of block length l/h. (a) Resonant frequencies, (b) damping of quasi-trapped-mode resonances and (c) damping of highly damped resonances. The asterisks denote BEM results of Rim & Kim (2000) for $l/h = 3$. $p = 8$, $d_{PML} = 2$, $\sigma_0 = 2$, $\Delta = 0.2$.

to the trapped modes becoming complex resonances for off-centre symmetric obstacles or obstacles asymmetric in y. In the following, we shall show that the narrowband attenuation is due to Fano resonances near the trapped-mode frequencies and for this purpose we compute again the resonances before treating the scattering problem.

4.1. *Resonances of rectangular screens in a duct*

As another example of a symmetric obstacle, we compute the resonances of a rectangular screen of length $l/h = 3$ and thickness $b/h = 0.5$, the parameters considered by Rim & Kim (2000), and vary the off-centre distance s/h sketched in figure 10(a). The results are shown in figure 11 for $0 \leqslant s/h < 0.3$. For $s/h = 0$ the rectangular block is centred and truly trapped modes exist with zero damping as demonstrated by Evans & Linton (1991). With $l/h = 3$ three trapped modes $n = 0, 1, 2$ exist below the cutoff frequency of the first crossmode $r = 1$, marked by the dotted line in figure 11(a). Here n denotes the number of modal nodes in the axial direction and solid curves denote x-symmetric modes and dashed curves x-antisymmetric modes. For $s/h \neq 0$, the resonant frequencies $\mathrm{Re}(K/2\pi)$ of the quasi-trapped modes (shown by solid symbols) as well as the strongly damped modes (marked by open symbols) increase only slightly with s/h. Rim & Kim (2000) found a similar trend for the frequency of the peak transmission loss in their parametric analysis of figure 16(c). This is also very similar to the results for the trapped-mode frequencies of an

https://doi.org/10.1017/S0022112010003757 Published online by Cambridge University Press

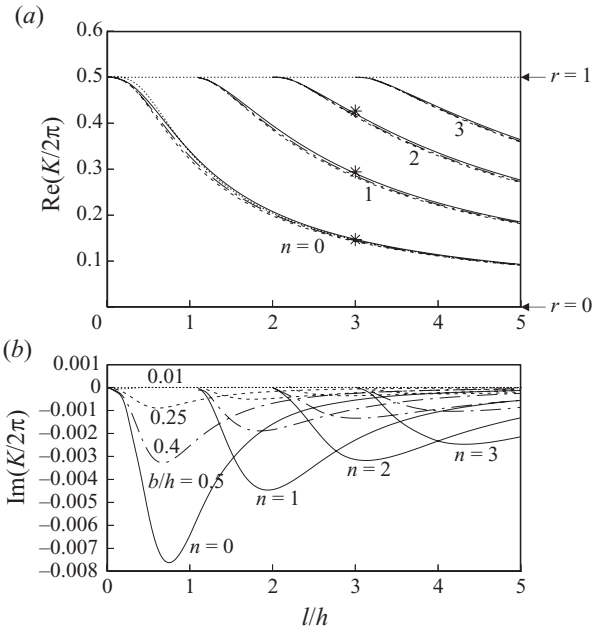


FIGURE 13. Acoustic resonances $n = 0, \ldots, 3$ of a rectangular block with $s/h = 0.15$ in a two-dimensional duct of width h: effect of block width b/h on the quasi-trapped-mode resonances. (a) Resonant frequency and (b) damping. The asterisks denote BEM results of Rim & Kim (2000) for peak transmission loss. $p = 8$, $d_{PML} = 4$, $\sigma_0 = 2$, $\Delta = 0.2$.

off-centred infinitely thin plate depicted in figure 2 of Evans, Linton & Ursell (1993). The asterisks in figure 11(a) show the frequencies of the peak transmission loss extracted from figure 7(b) of Rim & Kim (2000) assuming $c_0 = 340\,\mathrm{m\,s^{-1}}$. For $s/h = 0.25$, the rectangular block corresponds to a rectangular protrusion of the duct wall, a case for which McIver & Linton (1995) proved the non-existence of trapped modes.

Next, we investigate the influence of the screen length l/h in figure 12. Figure 12(a) shows the resonant frequencies $\mathrm{Re}(K/2\pi)$, whereas figures 12(b) and 12(c) show the damping $\mathrm{Im}(K/2\pi)$ of the quasi-trapped and highly damped modes, respectively. The former are marked by solid symbols and the latter by open symbols as in figure 11. Here circles denote x-symmetric modes and triangles denote x-antisymmetric modes. We note the large difference in damping between the quasi-trapped and highly damped modes in figures 12(b) and 12(c). Rim & Kim (2000) showed in their figure 16(e) that l/h is the most important tuning parameter because the frequency $\mathrm{Re}(K/2\pi)$ drops rapidly with increasing l/h. The asterisks in figure 12(a) show again the frequencies of the peak transmission loss at $l/h = 3$ extracted from figure 7(b) of Rim & Kim (2000). The frequencies of the quasi-trapped modes are always below the cutoff frequency $r = 1$ of the first crossmode, whereas the frequencies of the highly damped resonances seem to end at the cutoff frequency of the second symmetric duct mode $r = 2$.

Finally, in figure 13 we investigate the influence of the block width b/h on the first four quasi-trapped resonances keeping $s/h = 0.15$ constant. We observe that the resonant frequencies $\mathrm{Re}(K/2\pi)$ change very little with block width b/h in accordance with the findings of Rim & Kim (2000) in their figure 16(e). But the damping $\mathrm{Im}(K/2\pi)$ diminishes with decreasing block width and for $b/h = 0.01$ is very close to

https://doi.org/10.1017/S0022112010003757 Published online by Cambridge University Press

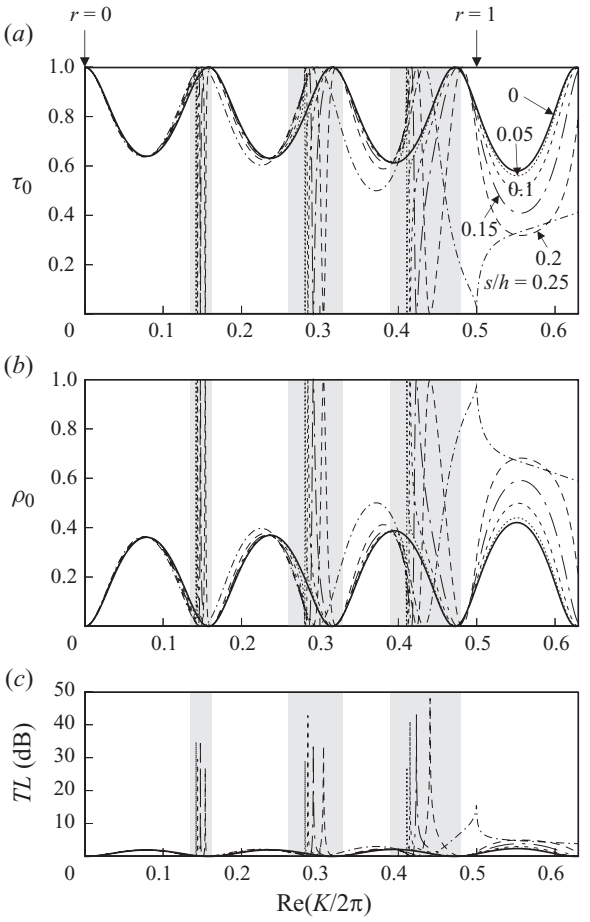


FIGURE 14. Transmission and reflection coefficients of a rectangular block with $l/h = 3$ and $b/h = 0.5$ in a two-dimensional duct of width h: effect of off-centre distance s/h. (a) Transmission coefficient τ_0, (b) reflection coefficient ρ_0 and (c) transmission loss TL. The frequency ranges near the Fano resonances are shaded.

the zero radiation loss of a truly trapped mode. Near the cutoff frequency of the first crossmode at $\mathrm{Re}(K/2\pi) = 0.5$, it is difficult to distinguish the resonant mode from the modes of the continuous spectrum in our numerical method, even for increased $\sigma_0 = 8$ and $d_{PML} = 10$. The asterisks at $l/h = 3$ in figure 13(a) show the frequency of peak transmission loss extracted from figure 7(b) of Rim & Kim (2000).

4.2. *Reflection and transmission coefficients of rectangular screens in a duct*

Again we start with a rectangular screen being centred in the duct, i.e. $s/h = 0$. The results are shown by the thick solid curve in figure 14. Here figure 14(a) gives the transmission coefficient τ_0, figure 14(b) gives the reflection coefficient ρ_0 and figure 14(c) gives the transmission loss TL. From figure 11 we see that for $s/h = 0$ we have three truly trapped-mode resonances below the cutoff frequency of the first duct crossmode each with a highly damped y-symmetric resonance nearby. From figure 12 we observe that above the cutoff frequency of the first duct crossmode, only highly damped resonances exist. Because the truly trapped-mode resonances cannot

https://doi.org/10.1017/S0022112010003757 Published online by Cambridge University Press

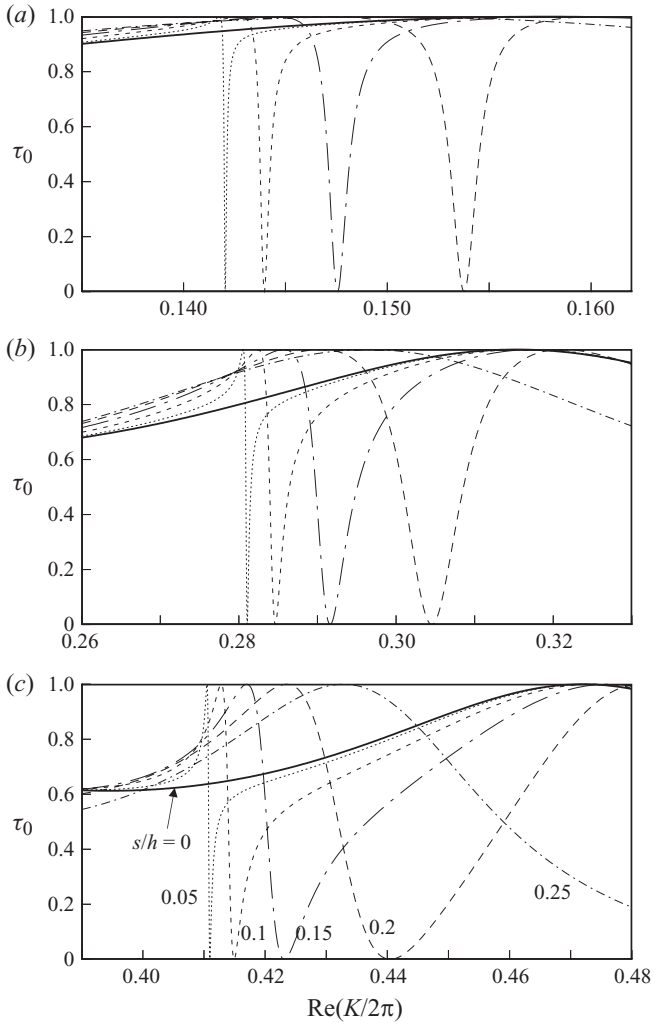


FIGURE 15. Expanded view of the transmission coefficients τ_0 in the three shaded regions of figure 14.

be excited by the fundamental duct mode, the transmission maxima of the solid thick curve in figure 14(a) are all due to the highly damped resonances.

With $s/h \neq 0$, the trapped modes become highly localized quasi-trapped modes which are the cause of the Fano resonances at frequencies slightly below the resonant frequencies of the damped modes. The narrow frequency ranges of the three Fano resonances are shaded in figure 14 and the transmission coefficients τ_0 in this range are reshown enlarged in figure 15. Clearly visible is the asymmetric line shape of the Fano resonances about the $s/h = 0$ curve with a transmission minimum following a transition maximum. The frequencies of the transmission maxima and minima increase slightly with increasing s/h. From figure 11 we see that the first two quasi-trapped modes cease to exist at $s/h = 0.25$, where the rectangular screen touches the sidewall of the duct. The third quasi-trapped-mode resonance $n = 2$ seems to become a highly damped resonance and continues beyond $s/h = 0.25$. As a consequence there are no more Fano resonances for the first two quasi-trapped

https://doi.org/10.1017/S0022112010003757 Published online by Cambridge University Press

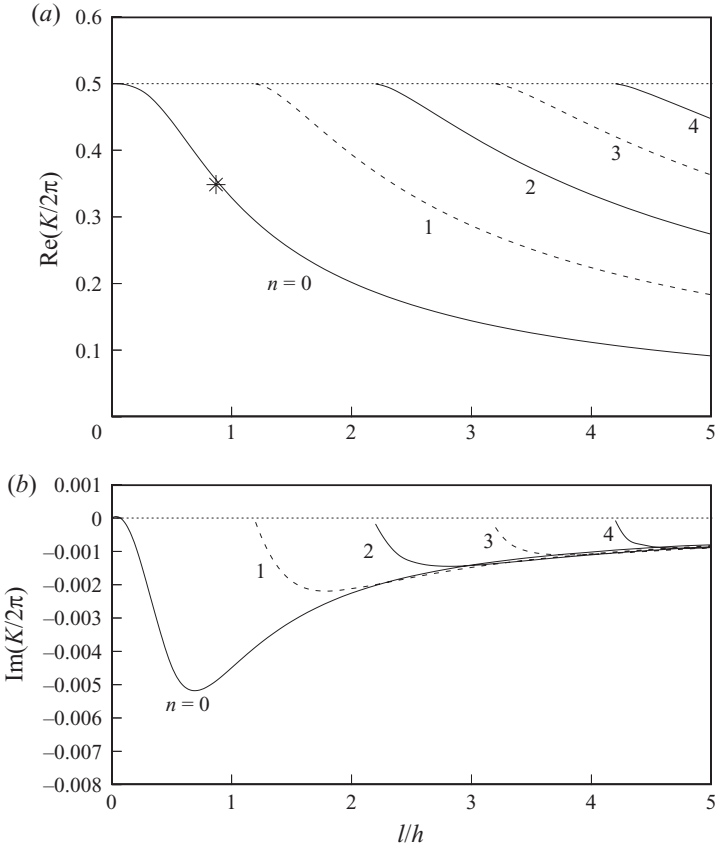


FIGURE 16. Acoustic resonances of a wedge with $b_1/h=0$, $b_2/h=0.5$ and $s/h=0.25$ centred in a two-dimensional duct of width h: effect of wedge length l/h: (a) resonant frequency and (b) damping. The asterisk denotes the experimental results of Rim & Kim (2000) for $l/h=0.87$. $p=6$, $d_{PML}=2(12)$, $\sigma_0=2$, $\Delta=0.2$.

modes in figures 14 and 15 if $s/h \geqslant 0.25$. The transmission loss plotted in figure 14(c) can be compared with the BEM results of Rim & Kim (2000) in their figure 12 (the cutoff frequency of the first duct crossmode in their rectangular duct of 9 cm $\times$ 10 cm is 1715 Hz).

4.3. *Resonances of wedges in a duct*

A second screen geometry investigated by Rim & Kim (2000) is a one-sided wedge with $b_1/h=0$ and $b_2/h=0.5$ centred on the duct axis, i.e. $s=0.25$, where now s is measured from the bottom wall as sketched in figure 10(b). The wedge is an example of an obstacle which is nonsymmetric in y and we show the corresponding quasi-trapped-mode resonances for variable wedge length l/h in figure 16. Again, more and more resonances n appear with increasing wedge length l/h starting at the cutoff frequency $\mathrm{Re}(K/2\pi)=0.5$ of the first duct crossmode. With increasing l/h the frequency decreases rapidly and the damping decreases steadily after reaching a maximum. The asterisk in figure 16(a) marks the experimental result of Rim & Kim (2000) for the peak transmission loss for a wedge with $l/h=0.87$ extracted from their figure 4. For $l/h=0.87$, only one quasi-trapped mode is excited as can be seen in

https://doi.org/10.1017/S0022112010003757 Published online by Cambridge University Press

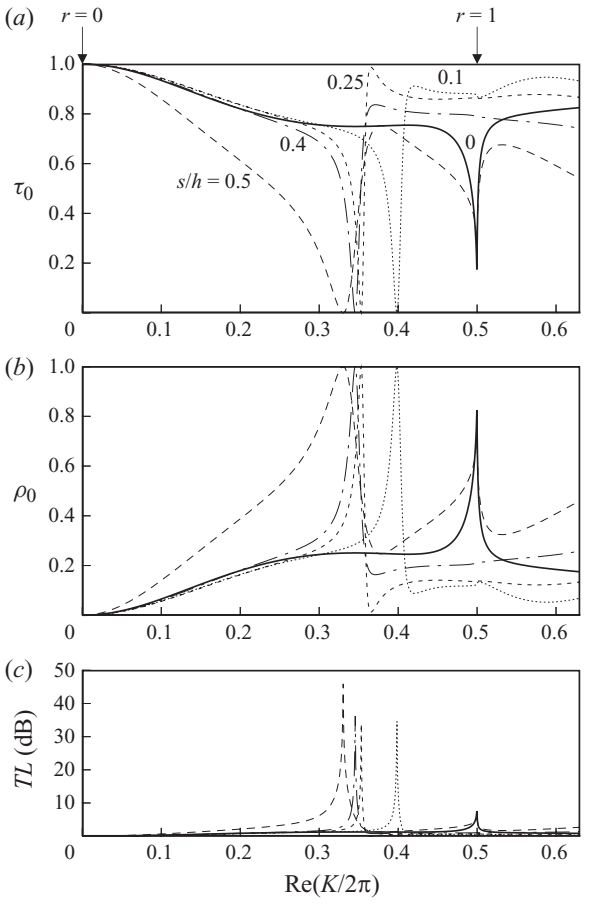


FIGURE 17. Transmission and reflection coefficients for a wedge with $b_1/h = 0$, $b_2/h = 0.5$ and $l/h = 0.87$ in a two-dimensional duct of width h: effect of varying s/h. (a) Transmission coefficient τ_0, (b) reflection coefficient ρ_0 and (c) transmission loss TL.

figure 16(a). For $l/h = 2$, the example treated theoretically by Rim & Kim (2000) in their figure 15, two quasi-trapped modes exist.

4.4. *Reflection and transmission coefficients of non-symmetric obstacles*

Using the geometry of the wedge investigated by Rim & Kim (2000), namely $b_1/h = 0$, $b_2/h = 0.5$ and $l/h = 0.87$, we first compute the transmission and reflection coefficients ρ_0 and τ_0, respectively, as well as the transmission loss TL for the centred wedge with $s/h = 0.25$. The results are shown in figure 17. Clearly, a Fano resonance is excited near the quasi-trapped-mode frequency even though the wedge is centred. Varying s/h between the two limiting cases $s/h = 0$ and $s/h = 0.5$ where the wedge touches the lower or upper duct wall respectively, we also see that the transmission maximum is visibly below 1. The transmission loss TL for $s/h = 0.1, 0.25$ and 0.4 can be compared with the experimental results of Rim & Kim (2000) for $y = 1, 2.5$ and 4 cm in their figure 4. The transmission coefficient τ_0 is the same whether the incoming wave impinges from the left or from the right as long as the frequency is below the cutoff frequency of the first duct crossmode. This is a consequence of the

https://doi.org/10.1017/S0022112010003757 Published online by Cambridge University Press

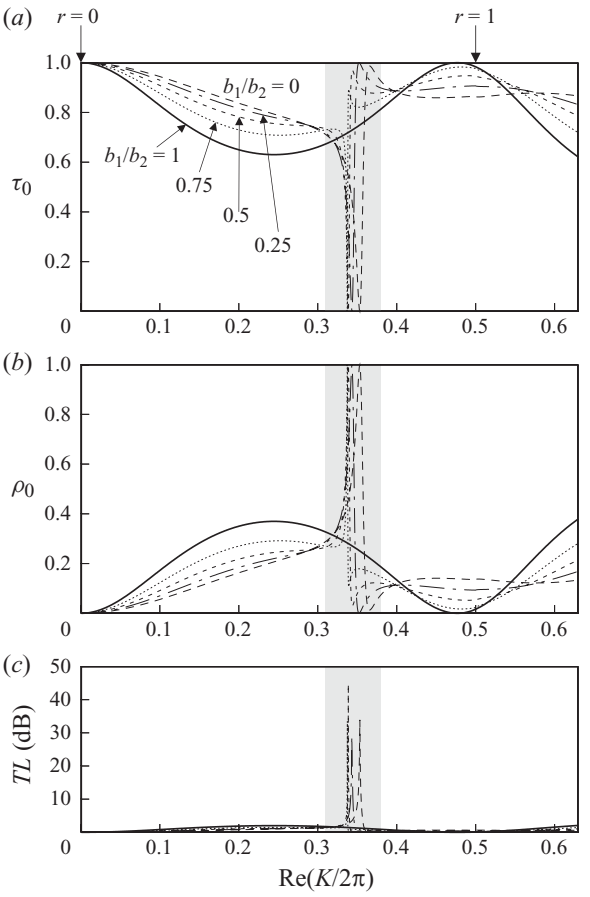


FIGURE 18. Transmission and reflection coefficients for a trapezoidal obstacle with $b_2/h = 0.5$, $l/h = 0.87$ and $s/h = 0.25$ in a two-dimensional duct of width h: effect of varying b_1/b_2. (a) Transmission coefficient τ_0, (b) reflection coefficient ρ_0 and (c) transmission loss TL. The frequency range near the Fano resonances is shaded.

reciprocity theorem which states that

$$\tau_{n;m} = \tau'_{m;n}. \tag{4.1}$$

Here $\tau_{n;m}$ denotes the modal energy transmission coefficient for an incoming wave impinging from the left and $\tau'_{m;n}$ for an incoming wave impinging from the right. Therefore, $\tau_{0;0} = \tau'_{0;0}$, which explains our numerical findings.

To see how the transmission coefficient changes from that for a centred rectangular screen where there is no Fano resonance (in physics some authors speak of 'ghost Fano resonance' in this situation; see for example Ladrón de Guevara, Claro & Orellana 2003) to that for the wedge investigated by Rim & Kim (2000), we vary b_1/h of the asymmetrical screen sketched in figure 10(b) keeping $l/h = 0.87$, $b_2/h = 0.5$ and $s/h = 0.25$ fixed. The results are shown in figure 18, with a more detailed view in figure 19 of the shaded Fano region of figure 18. We see that even though the screen is centred, Fano resonances appear as soon as the obstacle becomes nonsymmetric, i.e. $b_1 \neq b_2$. Again a transmission minimum occurs before the

https://doi.org/10.1017/S0022112010003757 Published online by Cambridge University Press

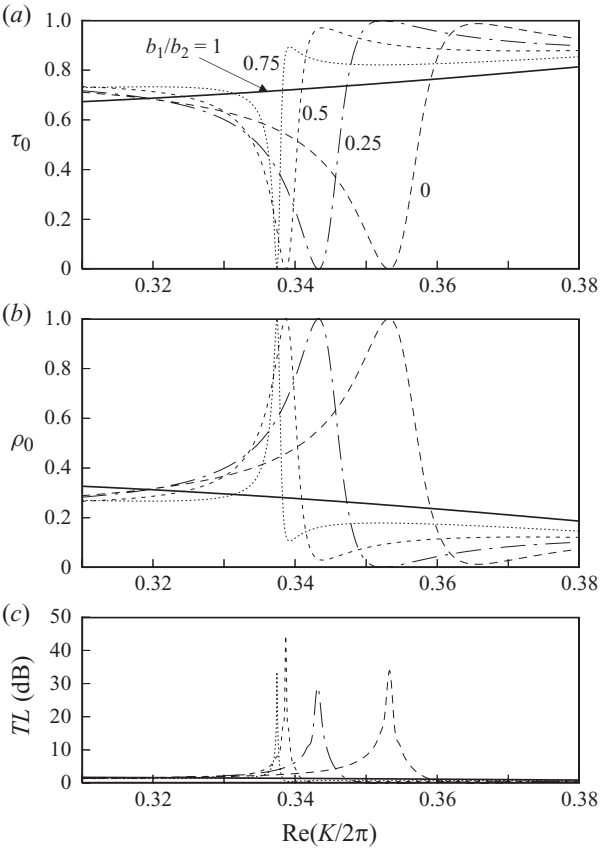


FIGURE 19. Expanded view of the frequency range $0.31 \leqslant \mathrm{Re}(K/2\pi) \leqslant 0.38$ shaded in figure 18. (*a*) Transmission coefficient τ_0, (*b*) reflection coefficient ρ_0 and (*c*) transmission loss TL.

transmission maximum contrary to the Fano resonances for an off-centre symmetrical obstacle. The transmission maxima are also visibly below 1 in most cases.

5. Conclusions

In this paper we performed a numerical study of acoustic resonances and scattering of sound by various obstacles in a two-dimensional duct without mean flow. The resonances are found as non-trivial solutions of the homogeneous problem (no incoming wave) satisfying vanishing Neumann boundary conditions on the duct walls and the scattering object in addition to the radiation condition that energy is radiated away from the scattering objects. This leads to a linear eigenvalue problem which is solved via the FEM in conjunction with two different types of absorbing boundary conditions, namely the complex scaling method and the Hardy space method. For symmetrical obstacles located on the centreline of the duct and an incoming plane wave, only the damped resonances, symmetric about the centreline of the duct, can be excited due to symmetry constraints. The maxima in the energy transmission coefficient are closely related to the resonances but, as far as we know, cannot be computed directly from the resonances.

Truly trapped modes with nominally zero radiation loss exist for symmetric geometries but can only be excited by localized sources such as self-excited vortices if

https://doi.org/10.1017/S0022112010003757 Published online by Cambridge University Press

mean flow is present. If the symmetry of the problem is broken, truly trapped modes become highly localized quasi-trapped modes. Opening up a second transmission path these quasi-trapped modes can interact resonantly with propagating duct modes generating narrowband Fano resonances with resonance and antiresonance features. It is shown that these Fano resonances can drastically change the transmission and reflection properties of plane waves. This opens up interesting applications in noise control with Fuller & Bies (1978) being an early example. Unfortunately, the reflection resonance occurs only over a rather narrow frequency range and if mean flow is present, the vortex shedding noise probably predominates over the reflection resonance.

We sincerely thank Joachim Schöberl and Thorsten Hohage for fruitful and stimulating discussions. The third author (L. N.) gratefully acknowledges financial support by the Deutsche Forschungsgemeinschaft (DFG) under grant Ho 2551/5-1. Furthermore, we are grateful to the three referees for their helpful suggestions.

REFERENCES

Aguilar, J. & Combes, J. M. 1971 A class of analytic perturbations for one-body Schrödinger Hamiltonians. *Commun. Math. Phys.* **22**, 269–279.

Al-Naib, I. A. I., Jansen, C. & Koch, M. 2009 High Q-factor metasurfaces based on miniaturized asymmetric single split resonators. *Appl. Phys. Lett.* **94**, 153505-1–153505-4.

Aly, K. & Ziada, S. 2010 Numerical simulation of internal cavities acoustic trapped modes with mean flow. In *ASME 3rd Joint US–European Fluids Engineering Summer Meeting and 8th International Conference on Nanochannels, Microchannels and Minichannels* – 1–5 August 2010, Montreal, Canada. ASME.

Aslanyan, A., Parnovski, L. & Vassiliev, D. 2000 Complex resonances in acoustic waveguides. *Q. J. Mech. Appl. Math.* **53**, 429–447.

Baslev, E. & Combes, J. M. 1971 Spectral properties of many body Schrödinger operators with dilation analytic interactions. *Commun. Math. Phys.* **22**, 280–294.

Bérenger, J. P. 1994 A perfectly matched layer for the absorption of electromagnetic waves. *J. Comput. Phys.* **114**, 185–200.

Bindel, D. S. & Govindjee, S. 2005 Elastic PMLs for resonator anchor loss simulation. *Intl J. Numer. Meth. Engng* **64**, 789–818.

Blevins, R. D. 1986 Acoustic modes of heat exchanger tube bundles. *J. Sound Vib.* **109** (3), 19–31.

Borthwick, D. 2007 *Spectral Theory of Infinite-Area Hyperbolic Surfaces*. Birkhäuser.

Boström, A. 1980 Transmission and reflection of acoustic waves by an obstacle in a waveguide. *Wave Motion* **2**, 167–184.

Callan, M., Linton, C. M. & Evans, D. V. 1991 Trapped modes in two-dimensional waveguides. *J. Fluid Mech.* **229**, 51–64.

Cattapan, G. & Lotti, P. 2007 Fano resonances in stubbed quantum waveguides with impurities. *Eur. Phys. J.* B **60**, 51–60.

Chew, W. C. & Weedon, W. H. 1994 A 3-D perfectly matched medium from modified Maxwell's equation with stretched coordinates. *Microw. Opt. Technol. Lett.* **7** (13), 599–604.

Cobelli, P. J., Pagneux, V., Maurel, A. & Petitjeans, P. 2009 Experimental observation of trapped modes in a water wave channel. *EPL* **88**, 20006-p1–20006-p6.

Collino, F. & Monk, P. 1998 The perfectly matched layer in curvilinear coordinates. *SIAM J. Sci. Comput.* **19** (6), 2061–2090.

Davies, E. B. & Parnovski, L. 1998 Trapped modes in acoustic waveguides. *Q. J. Mech. Appl. Math* **51**, 477–492.

Duan, Y., Koch, W., Linton, C. M. & McIver, M. 2007 Complex resonances and trapped modes in ducted domains. *J. Fluid Mech.* **571**, 119–147.

El Boudouti, E. H., Mrabti, T., Al-Wahsh, H., Djafari-Rouhani, B., Akjouj, A. & Dobrzynski, L. 2008 Transmission gaps and Fano resonances in an acoustic waveguide: analytical model. *J. Phys. Condens. Matter.* **20**, 255212-1–255212-10.

https://doi.org/10.1017/S0022112010003757 Published online by Cambridge University Press

Evans, D. V. 1992 Trapped acoustic modes. *IMA J. Appl. Math.* **49** (1), 45–60.

Evans, D. V., Levitin, M. & Vassiliev, D. 1994 Existence theorems for trapped modes. *J. Fluid Mech.* **261**, 21–31.

Evans, D. V. & Linton, C. M. 1991 Trapped modes in open channels. *J. Fluid Mech.* **225**, 153–175.

Evans, D. V., Linton, C. M. & Ursell, F. 1993 Trapped mode frequencies embedded in the continuous spectrum. *Q. J. Mech. Appl. Math.* **46**, 253–274.

Evans, D. V. & Porter, R. 1997 Trapped modes about multiple cylinders in a channel. *J. Fluid Mech.* **339**, 331–356.

Evans, D. V. & Porter, R. 1998 Trapped modes embedded in the continuous spectrum. *Q. J. Mech. Appl. Math.* **52**, 263–274.

Evans, D. V. & Porter, R. 1999 Trapping and near-trapping by arrays of cylinders in waves. *J. Engng Math.* **35**, 149–179.

Fano, U. 1935 Sullo spettro di assorbimento dei gas nobili presso il limite dello spettro d'arco. *Nuovo Cimento* **12**, 154–161.

Fano, U. 1961 Effects of configuration interaction on intensities and phase shifts. *Phys. Rev.* **124** (6), 1866–1878.

Fano, U., Pupillo, G., Zannoni, A. & Clark, C. W. 2005 On the absorption spectrum of noble gases at the arc spectrum limit. *J. Res. Natl. Inst. Stand. Technol.* **110**, 583–587.

Fedotov, V. A., Rose, M., Prosvirnin, S. L., Papasimakis, N. & Zheludev, N. I. 2007 Sharp trapped-mode resonances in planar metamaterials with a broken structural symmetry. *Phys. Rev. Lett.* **99**, 147401-1–147401-4.

Fuller, C. R. & Bies, D. A. 1978 A reactive acoustic attenuator. *J. Sound Vib.* **56**, 45–59.

Harari, I., Patlashenko, I. & Givoli, D. 1998 Dirichlet-to-Neumann maps for unbounded wave guides. *J. Comp. Phys.* **143**, 200–223.

Hein, S., Hohage, T. & Koch, W. 2004 On resonances in open systems. *J. Fluid Mech.* **506**, 255–284.

Hein, S., Hohage, T., Koch, W. & Schöberl, J. 2007 Acoustic resonances in a high lift configuration. *J. Fluid Mech.* **582**, 179–202.

Hein, S. & Koch, W. 2008 Acoustic resonances and trapped modes in pipes and tunnels. *J. Fluid Mech.* **605**, 401–428.

Hislop, P. D. & Sigal, I. M. 1996 *Introduction to Spectral Theory*. Springer.

Hohage, T. & Nannen, L. 2009 Hardy space infinite elements for scattering and resonance problems. *SIAM J. Numer. Anal.* **47** (2), 972–996.

Hu, F. Q. 2004 Absorbing boundary conditions. *Intl J. Comput. Fluid Dyn.* **18** (6), 513–522.

Joe, Y. S., Satanin, M. & Kim, C. S. 2006 Classical analogy of Fano resonances. *Phys. Scr.* **74**, 259–266.

Kim, S. & Pasciak, J. E. 2009 The computation of resonances in open systems using a perfectly matched layer. *Math. Comput.* **78**, 1375–1398.

Kirby, R. 2008 Modelling sound propagation in acoustic waveguides using a hybrid numerical method. *J. Acoust. Soc. Am.* **124** (4), 1930–1940.

Koch, W. 2009 Acoustic resonances and trapped modes in annular plate cascades. *J. Fluid Mech.* **628**, 155–180.

Ladrón de Guevara, M. L., Claro, F. & Orellana, P. A. 2003 Ghost Fano resonance in a double quantum dot molecule attached to leads. *Phys. Rev.* B **67**, 195335-1–195335-6.

Li, Y. & Mei, C. C. 2006 Subharmonic resonance of a trapped wave near a vertical cylinder in a channel. *J. Fluid Mech.* **561**, 391–416.

Linton, C. M. 1995 Acoustic scattering by a sphere in a circular cylindrical waveguide. *Q. J. Mech. Appl. Math.* **48**, 211–235.

Linton, C. M. & Evans, D. V. 1992 The radiation and scattering of surface waves by a vertical circular cylinder in a channel. *Phil. Trans. R. Soc. Lond.* A **338**, 325–357.

Linton, C. M. & McIver, M. 2002 Periodic structures in waveguides. *Proc. R. Soc. Lond.* A **458**, 3003–3021.

Linton, C. M., McIver, M., McIver, P., Ratcliffe, K. & Zhang, J. 2002 Trapped modes for off-centre structures in guides. *Wave Motion* **36**, 67–85.

McIver, M. & Linton, C. M. 1995 On the non-existence of trapped modes in acoustic waveguides. *Q. J. Mech. Appl. Math.* **48**, 543–555.

https://doi.org/10.1017/S0022112010003757 Published online by Cambridge University Press

Mingaleev, S. F., Miroshnichenko, A. E. & Kivshar, Y. S. 2008 Coupled-resonator-induced reflection in photonic-crystal waveguides. *Opt. Express* **16**, 11647–11659.

Miroshnichenko, A. E., Flach, S. & Kivshar, Y. S. 2010 Fano resonances in nanoscale structures. *Rev. Mod. Phys.* **82**, 2257–2298.

Moiseyev, N. 1998 Quantum theory of resonances: calculating energies, widths and cross-sections by complex scaling. *Phy. Rep.* **302**, 211–293.

Nannen, L. 2008 Hardy-Raum Methoden zur numerischen Lösung von Streu- und Resonanzproblemen auf unbeschränkten Gebieten. PhD thesis, Georg-August Universität Göttingen, Der Andere Verlag, Tönning.

Nannen, L. & Schädle, A. 2010 Hardy space infinite elements for Helmholtz-type problems with unbounded inhomogeneities. arXiv:math.NA/1025v1.

Papasimakis, N., Fedotov, V. A. & Zheludev, N. I. 2008 Metamaterial analog of electromagnetically induced transparency. *Phys. Rev. Lett.* **101**, 253903-1–253903-4.

Parker, R. 1978 Acoustic resonances in passages containing banks of heat exchanger tubes. *J. Sound Vib.* **57**, 245–260.

Parker, R. 1984 Acoustic resonances and blade vibration in axial flow compressors. *J. Sound Vib.* **92**, 529–539.

Parker, R. & Stoneman, S. A. T. 1989 The excitation and consequences of acoustic resonances in enclosed fluid flow around solid bodies. *Proc. Inst. Mech. Engng* **203**, 9–19.

Pierce, A. D. 1981 *Acoustics*. McGraw Hill.

Porter, R. 2007 Trapped modes in thin elastic plates. *Wave Motion* **45**, 3–15.

Porter, R. & Evans, D. V. 1999 Rayleigh–Bloch surface waves along periodic gratings and their connection with trapped modes in waveguides. *J. Fluid Mech.* **386**, 233–258.

Porter, R. & Evans, D. V. 2002 Trapped modes about tube bundles in waveguides. In *IUTAM Symposium on Diffraction in Fluid Mechanics and Elasticity* (ed. P. A. Martin, I. D. Abrahams & M. J. Simon), pp. 87–94. Kluwer.

Retzler, C. H. 2001 Trapped modes: an experimental investigation. *Appl. Ocean Res.* **23** (4), 249–250.

Rim, M. & Kim, Y.-H. 2000 Narrowband noise attenuation characteristics of in-duct acoustic screens. *J. Sound Vib.* **234** (5), 737–759.

Schöberl, J. 1997 NETGEN: an advancing front 2D/3D-mesh generator based on abstract rules. *Comput. Vis. Sci.* **1**, 41–52.

Shao, Z.-A., Porod, W. & Lent, C. S. 1994 Transmission resonances and zeros in quantum waveguide systems with attached resonators. *Phys. Rev.* B **49** (11), 7453–7465.

Simon, B. 1973 The theory of resonances for dilation analytic potentials and the foundations of time-dependent perturbation theory. *Ann. Math.* **97**, 247–274.

Utsunomiya, T. & Eatock Taylor, R. 1999 Trapped modes around a row of circular cylinders in a channel. *J. Fluid Mech.* **386**, 259–279.

Voo, K.-K. & Chu, C. S. 2006 Localized states in continuum in low-dimensional systems. *Phys. Rev.* B **74**, 155306-1–155306-7.

Zworski, M. 1999 Resonances in physics and geometry. *Not. AMS* **46** (3), 319–328.

https://doi.org/10.1017/S0022112010003757 Published online by Cambridge University Press